

Measurement of the baryonic acoustic oscillation scale in 21 cm intensity fluctuations during the reionisation era

Kirsty J. Rhook^{1*}, Paul M. Geil^{2†} & J. Stuart B. Wyithe^{2‡}

¹*Institute of Astronomy, Madingley Road, Cambridge CB3 0HA*

²*School of Physics, University of Melbourne, Parkville, Victoria, Australia*

Draft Version March 18th, 2008

ABSTRACT

It has recently been suggested that the power spectrum of redshifted 21 cm fluctuations could be used to measure the scale of baryonic acoustic oscillations (BAOs) during the reionisation era. The resulting measurements are potentially as precise as those offered by the next generation of galaxy redshift surveys at lower redshift. However unlike galaxy redshift surveys, which in the linear regime are subject to a scale independent galaxy bias, the growth of ionised regions during reionisation is thought to introduce a strongly scale dependent relationship between the 21 cm and mass power spectra. We use a semi-numerical model for reionisation to assess the impact of ionized regions on the precision and accuracy with which the BAO scale could be measured using redshifted 21 cm observations. For a model in which reionisation is completed at $z \sim 6$, we find that the constraints on the BAO scale are not systematically biased at $z \gtrsim 6.7$. Assuming the sensitivity attainable with a low-frequency array comprising 10 times the collecting area of the Murchison Widefield Array, the BAO scale could be measured to within 1.5 per cent in the range $6.7 \lesssim z \lesssim 8$.

Key words: cosmology: diffuse radiation – large-scale structure of the universe

1 INTRODUCTION

The imprint of baryonic acoustic oscillations (BAOs) on the mass power spectrum (PS) provides a cosmic yardstick that can be used to measure the dependence of both the angular diameter distance and Hubble parameter on redshift. The wavelength of a BAO is related to the size of the sound horizon at recombination. Its value depends on the Hubble constant, and on the dark matter and baryon densities. However, it does not depend on the amount or nature of dark energy. Thus measurements of the angular diameter distance and Hubble parameter can in turn be used to constrain the possible evolution of dark energy with cosmic time (e.g. Eisenstein et al. 1998; Eisenstein 2002).

Galaxy surveys have proven to be a powerful probe of the linear PS on large scales and therefore provide a means to measure the BAO scale (e.g. Blake & Glazebrook 2003; Seo & Eisenstein 2003, 2005; Glazebrook & Blake 2005; Hu & Haiman 2003; Seo & Eisenstein 2007; Angulo et al. 2008). Indeed, analyses of the galaxy PS from the SDSS and 2dFGRS surveys have uncovered a BAO signal (e.g. Cole et al. 2005; Eisenstein et al. 2005; Percival et al. 2007),

providing incentive for deeper all-sky galaxy surveys, using telescopes like the SKA¹, Pan-STARRS² and the LSST³, to measure the BAO scale and hence the dark energy equation of state more accurately.

Galaxy redshift surveys are best suited to studies of the dark energy equation of state at relatively late times ($z \lesssim 3$) due to the difficulty of obtaining accurate redshifts for a sufficiently large number of high redshift galaxies. Although detection of the Integrated Sachs-Wolfe effect puts some constraints on the integrated role of dark energy above $z \sim 1.5$ [see, e.g. Giannantonio et al. (2008) and references therein], we currently have very limited information about the nature of dark energy at high redshift. If dark energy behaves like a cosmological constant, then its effect on the Hubble expansion is only significant at $z \lesssim 1$ and becomes negligible at $z \gtrsim 2$. In this case, studies of the BAO scale at low redshift would provide the most powerful constraints. However, as the origin of dark energy is not understood we cannot presume a priori which redshift range should be studied in order to provide optimal constraints on proposed models. Probes of dark energy at higher redshifts have been suggested. These include measurements of the PS from a

* krhook@ast.cam.ac.uk

† pgeil@physics.unimelb.edu.au

‡ swyithe@unimelb.edu.au

¹ <http://www.skatelescope.org>

² <http://pan-starrs.ifa.hawaii.edu/public>

³ <http://www.lsst.org>

Ly α forest survey which could potentially be used probe the evolution of dark energy through measurement of the BAO scale for redshifts as high as $z \sim 4$ (McDonald & Eisenstein 2007). Similarly, studying the temporal variation of high resolution quasar spectra may probe the evolution of dark energy through the Sandage-Loeb test in the window $2 < z < 5$ (Corasaniti et al. 2007). Measurements of the BAO scale in the reionisation era ($z > 6$) are likely to be complimentary to the constraints at lower redshifts provided by these techniques.

It has recently been suggested that observations of 21 cm intensity fluctuations might provide an additional avenue to measure the mass PS (e.g. McQuinn et al. 2006; Bowman et al. 2006; Mao et al. 2008), and that future low-frequency arrays could be used to measure the BAO scale at a range of redshifts (Wyithe et al. 2008; Chang et al. 2007; Mao & Wu 2008). Redshifted 21 cm surveys are sensitive to neutral hydrogen regardless of whether it is part of a resolved object. As a result, at high redshifts such surveys may be more efficient in measuring the large-scale mass distribution than galaxy redshift surveys, which must identify a very large number of individual galaxies. Furthermore, spectroscopic emission line surveys have the advantage of probing a precisely defined redshift interval, which is unlikely to be true of a traditional galaxy survey (see Simpson & Bridle 2006).

Planned low-frequency arrays such as the Murchison Widefield Array⁴ (MWA) and LOFAR⁵ are designed to measure the PS of 21 cm fluctuations at $z > 6$ in order to probe the reionisation era. Wyithe et al. (2008) have argued that while the first generation of low-frequency arrays will not have sufficient sensitivity to precisely determine the BAO scale, future extensions could have the sensitivity to detect the BAO scale with promisingly small errors. Wyithe et al. (2008) assumed a semi-analytic model which predicts a scale independent value for the effective bias between the linear matter PS and the 21 cm PS. However the 21 cm bias is expected to be strongly scale dependent, especially toward the end of reionisation when many ionised bubbles percolate through the intergalactic medium (IGM), creating an excess of power on scales larger than the characteristic bubble size (e.g. Furlanetto et al. 2004). In this paper we explore whether the scale dependence of the 21 cm bias will compromise the ability of redshifted 21 cm observations to measure the BAO scale (Mao & Wu 2008). We begin by reviewing the expected BAO signal and 21 cm PS in Section 2. We describe the observation of the 21 cm PS, including a discussion of the noise considerations in Section 3. In Section 4 we describe our fitting procedure for recovering the BAO scale and present our error analysis, before concluding in Section 5.

2 THEORETICAL BACKGROUND

The sound speed at recombination (s) determines the length scale of the acoustic peaks in both the cosmic microwave background (CMB) anisotropies and the linear matter PS.

We refer to this length as the BAO scale. The co-moving horizon size at decoupling (r) may be determined from knowledge of Ω_m and Ω_b , and an understanding of the physics governing a baryon-photon fluid (Page et al. 2003). Komatsu et al. (2008) calculate this length scale to be 146 ± 1.8 Mpc for the cosmological parameters extracted from the fifth year WMAP data. The corresponding angular scale $\theta_A = s/D_A(z_{\text{rec}})$ is closely related to the position of the first acoustic peak in the CMB PS, which occurs at the scale of the mode which has compressed once at the time of decoupling (see Page et al. 2003). Following decoupling the same acoustic scale is imprinted in the matter PS, albeit with a different phase. This signature is expected to be preserved on large scales where non-linear gravitational effects are small. Therefore the BAO scale may be used as a standard ruler to test the geometry of the universe and the role of dark energy.

2.1 Theoretical expectations for the redshifted 21 cm power spectrum

Neutral hydrogen radiates at 21 cm due to the hyperfine transition between the singlet and triplet ground states. Assuming a contrast between the kinetic temperature of the IGM T_k and the CMB temperature T_{CMB} , and efficient coupling of the spin temperature T_s to T_k , the 21 cm signal will mirror the underlying density of neutral hydrogen. The Ly α and X-ray flux emitted by the first galaxies is expected to ensure these conditions hold during most of the reionisation era (see, e.g. Furlanetto 2006). A radio interferometer is sensitive to fluctuations in the brightness temperature of neutral gas. For gas of mean cosmic density the expected temperature brightness contrast in redshifted 21 cm emission is

$$\begin{aligned} \delta T_b &= \frac{T_b - T_{\text{CMB}}}{T_{\text{CMB}}(1+z)} \\ &\approx 22 \text{ mK } x_{\text{HI}} \left(1 - \frac{T_{\text{CMB}}}{T_s}\right) \left(\frac{\Omega_b h^2}{0.02}\right) \\ &\quad \left[\left(\frac{1+z}{7.5}\right) \left(\frac{0.24}{\Omega_m}\right)\right]^{1/2}, \end{aligned} \quad (1)$$

where x_{HI} is the mass-weighted neutral fraction of hydrogen in the IGM.

The 21 cm PS is related to the mass PS. Assuming spherical symmetry the 21 cm PS may be written as

$$P_{21}(k, z) = b_{21}(k, z)^2 P_l(k, z) D^2(z), \quad (2)$$

where P_l is the primordial linear matter PS extrapolated to $z = 0$ calculated using CMBfast (Seljak & Zaldarriaga 1996) assuming the third-year WMAP cosmological parameters (Spergel et al. 2007), and $D(z)$ is the linear growth factor between redshift z and the present. In writing equation (2) we assume that the gravitational dynamics governing the large-scale structures probed are well described by linearised fluid equations. Non-linear gravitational dynamics will be increasingly important at low redshift. However at the redshifts of interest here ($z > 6$) non-linear evolution is unlikely to play a significant role (see, e.g. Crocce & Scoccimarro 2008; Mao & Wu 2008). Mao et al. (2008) find that the cut-off in the maximum wave number probed by redshifted 21 cm

⁴ <http://www.haystack.mit.edu/ast/arrays/mwa>

⁵ <http://www.lofar.org>

PS in the range $7 < z < 9$ has little affect on the constraints on cosmological parameters.

In the early stages of reionisation when most of the hydrogen is still neutral, the bias between the linear matter PS and the 21 cm PS, b_{21} , is well approximated by a constant with units of temperature. However the bias is expected to depend on scale during to the process of reionisation since galaxies preferentially form in overdense regions, resulting in early formation of ionised bubbles from an overdense IGM. This effect can be modeled semi-analytically (e.g. Wyithe & Morales 2007), or with full numerical calculations of reionisation (e.g. McQuinn et al. 2007a,b; Trac & Cen 2007). Recently, semi-numerical schemes have been devised which allow efficient calculation of the large-scale ionisation field (Mesinger & Furlanetto 2007; Zahn et al. 2007; Geil & Wyithe 2007). We use simulations computed using the method described in Geil & Wyithe (2007) to model b_{21} .

2.2 Model for the evolution of the 21 cm signal

We refer the reader to the discussion of the semi-analytic model for the reionisation of the IGM by Wyithe & Morales (2007) and the corresponding semi-numerical calculation of the distribution of ionised gas by Geil & Wyithe (2007). Only a brief overview of the assumptions and characteristics of the model(s) is included here.

Wyithe & Morales (2007) describe a semi-analytic model for the density and scale dependent ionisation fraction of the IGM. This model assumes that a certain fraction of the mass in collapsed halos forms galaxies, and that these galaxies produce ionising photons with some efficiency. The ionisation due to galaxies is opposed by the density dependent recombination rate. An overdensity dependent rate of ionisation may then be calculated as a function of scale. The parameters of this model are tuned such that reionisation is completed by $z = 6$. Wyithe & Morales (2007) use this model to explore the 21 cm brightness temperature contrast as a function of scale and redshift. Geil & Wyithe (2007) use the scale and overdensity dependent predictions for the ionised gas fraction of the IGM to track realisations of the real-space density and ionisation fraction of a region of the IGM. We use this semi-numerical model to compute the 21 cm bias b_{21} . We note that our calculation does not include redshift space distortions (Barkana & Loeb 2005) which are not captured by the model used in this paper. The free parameters include the star formation efficiency, escape fraction of ionising photons, and the minimum halo virial temperature for star formation in neutral and ionised regions of IGM (for which we take 10^4 K and 10^5 K respectively). The semi-numerical simulation was performed in a cube with 256^3 resolution elements and of side length 3 Gpc (co-moving).

In Figure 1 we show model 21 cm PS at $z = 6.5, 7, 7.5$ and 8 . The left-hand panels show the ionised gas distribution from the semi-numerical simulations for a box with side length 3 Gpc (co-moving). The panels in the second column show the spherically averaged model 21 cm PS (grey lines). The panels in the third column show the model 21 cm bias (grey lines). The far right-hand panels show the BAO component of the PS, defined as the difference between the 21 cm PS, and a reference 21 cm PS computed from a mass PS without baryons, $P_{l,nb}(k)$. The model BAO component,

$b_{21}^2(k)D^2(z)[P_l(k) - P_{l,nb}(k)]$, is shown in grey. The model PS is reproduced in Figure 2.

2.3 Fitting formula for 21 cm power spectra

Following Seo & Eisenstein (2005) we parametrize the fit to the semi-numerical model of the spherically averaged 21 cm PS as

$$P_{21,\text{fit}}(k, z) = B^2(k) D^2(z) P_l(k/\alpha) + AP(k), \quad (3)$$

where $AP(k) = c_0 + c_1k + c_2k^2$ is a term to describe anomalous power and $B(k) = b_0 + b_1 + b_2k^2 + b_3k^3$ is the fitted bias in units of mK. The dilation parameter α allows for a dilation/contraction of the matter PS used to fit the 21 cm PS. In our case the input value of α is unity since we are assuming we know the cosmological parameters governing P_l . Seo & Eisenstein (2005) note that for the parametrization the PS in equation (3), the errors in the known values of the wave-number dilation parameter α directly translate into the errors in the measured BAO scales.

Our semi-numerical model is intrinsically linear, and so does not include anomalous power, which describes the modification of the PS due to non-linear evolution. However we explore the possible effect of anomalous power on measurement of the BAO scale by including the correction term AP in the fitted PS. Inclusion of this term approximates the effect of degeneracy between anomalous power and scale dependent bias. In this paper we present results using fits both with and without the AP term.

The 3d wave vector \vec{k} can be decomposed into components perpendicular k_\perp and parallel k_\parallel to the line-of-sight. The modulus of the wave number is $k = |\vec{k}| = \sqrt{k_\parallel^2 + k_\perp^2}$. Since a low-frequency array will measure both the line-of-sight and transverse components of the 21 cm PS (see Section 3), we may generalise equation (3) as

$$P_{21,\text{fit}}(k_\perp, k_\parallel, z) = B^2(\sqrt{k_\perp^2 + k_\parallel^2}) D^2(z) \times P_l(\sqrt{(k_\perp/\alpha_\perp)^2 + (k_\parallel/\alpha_\parallel)^2}) + AP(\sqrt{k_\perp^2 + k_\parallel^2}). \quad (4)$$

where $\alpha_\perp, \alpha_\parallel$ allow for a dilation in the measurement of the wave-number (and therefore BAO scale) in the transverse and line-of-sight components respectively. As described by Seo & Eisenstein (2005), we may interpret the errors in α_\perp and α_\parallel for our fits as the errors in the measurement of the transverse and line-of-sight BAO scales. We calculate the expected redshift dependent errors $\Delta\alpha_\perp$ and $\Delta\alpha_\parallel$ in Section 4.2 for the observations described below (Section 3).

3 MEASUREMENT OF 21 CM POWER SPECTRA

In this section we discuss the sensitivity of a low-frequency array to the 21 cm PS. The sensitivity to the PS depends on the array design (e.g. total collecting area and antenna distribution) as well as the observation strategy (e.g. total integration time). We consider a low-frequency array which would be a 10-fold extension of the MWA. We refer to this array as the MWA5000 (McQuinn et al. 2006). The MWA5000 would consist of 5000 antennae (with each

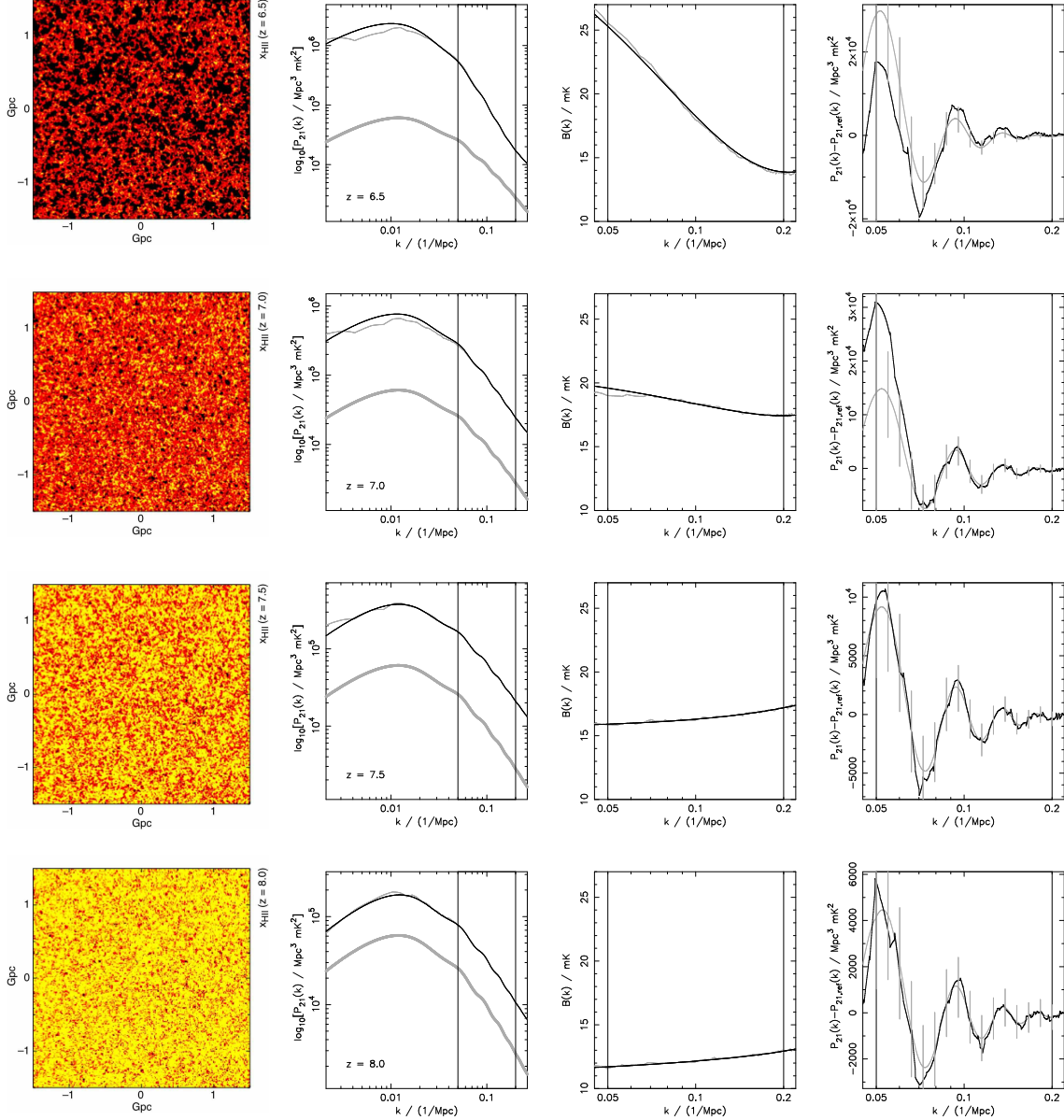


Figure 1. Model power spectra and fits assuming a third-order polynomial bias and no anomalous power. The left-hand panels show the ionisation maps corresponding to redshifts of $z = 6.5, 7.0, 7.5$ and 8.0 . The panels in the second column display the corresponding model (*grey*) and fitted (*black*) 21 cm PS, and the linear matter PS (*thick grey* line). The panels in the third column show the fitted (*black*) and model (*grey*) scale dependent bias. In the far right-hand panels we plot the difference between the model 21 cm PS with and without baryons (*grey*), and the recovered 21 cm PS with and without baryons (*black*), as described in the text. The *grey* error bars correspond to spherically averaged noise as described in Section 3. In each panel the vertical lines indicate the range of k values used for the fit.

antenna composed of a tile of 4×4 cross-dipoles) with effective collecting area $A_e \sim 16\lambda^2/4 \text{ m}^2$, where $\lambda = 0.21(1+z) \text{ m}$ is the observed wavelength. The dipoles will be sensitive to a wide range of frequencies which translate into redshifts spanning the expected extent of reionisation. However, we assume that the receiver will limit the bandpass to a selected $B_{\text{tot}} = 32 \text{ MHz}$ window per observation. We assume that the antennae are distributed with constant density in a core of radius 80 m (within which the u - v coverage is very high), with the remainder distributed with a radially symmetric density profile $\rho \propto r^{-2}$ out to a radius of 1 km (so that the maximum baseline is $\sim 2 \text{ km}$).

We use the prescription from Bowman et al. (2006) for the 3d sensitivity of an array to the 21 cm PS. The array sensitivity is expressed in terms of the wave vector components k_{\perp} and k_{\parallel} . The sensitivity at large k depends crucially on the angular resolution of the array (and therefore the maximum baseline), the bandpass over which the measurement is made $\Delta\nu$, the integration time t_{int} , and the density of baselines which measure a particular k -mode. The noise may be divided into two distinct components. The thermal noise component $\Delta P_{21,N}$ is proportional to the sky temperature, where $T_{\text{sky}} \sim 250 \left(\frac{1+z}{7}\right)^{2.6} \text{ K}$ at the frequencies of interest,

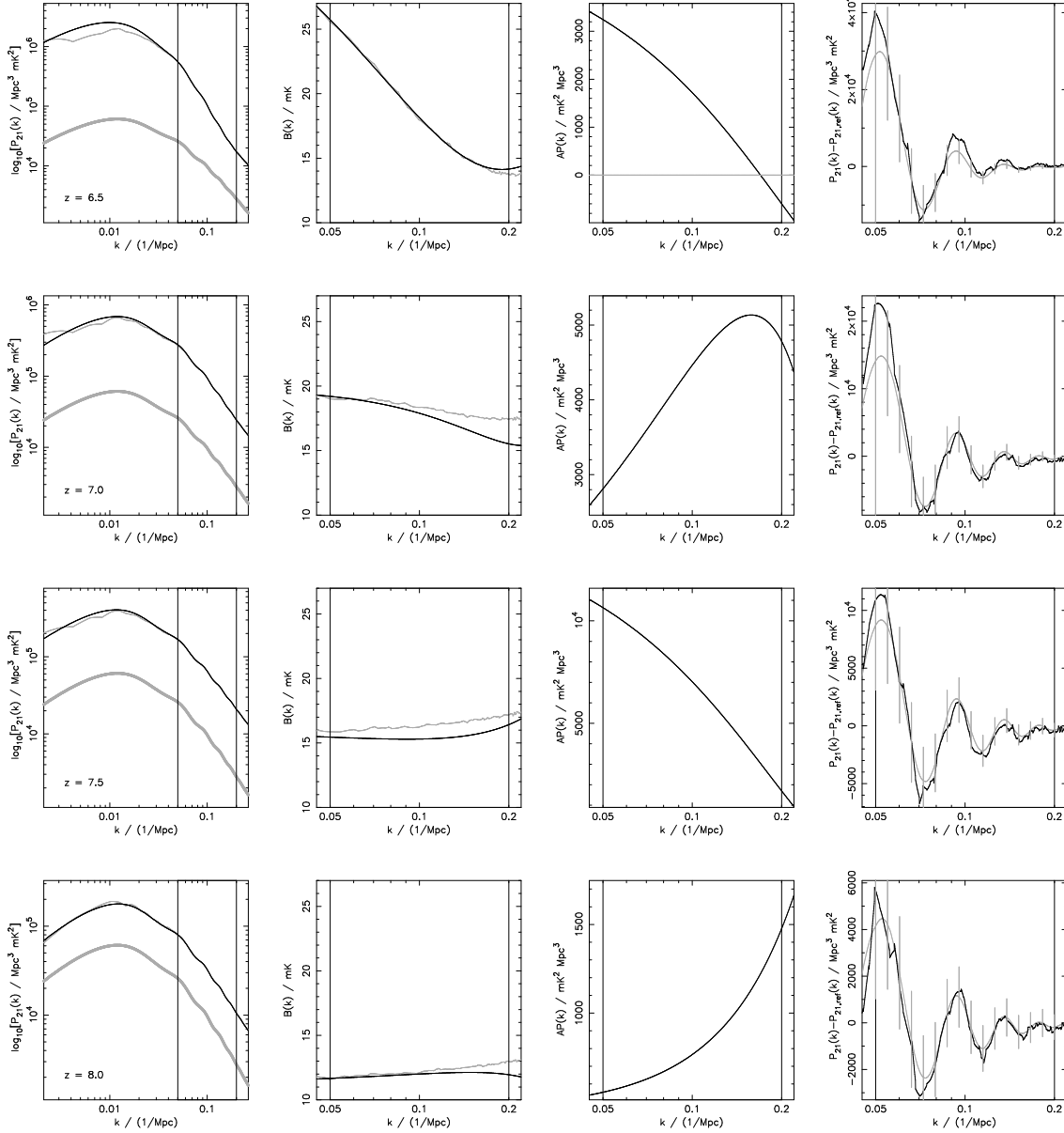


Figure 2. Model power spectra and fits assuming a third-order polynomial bias and quadratic anomalous power for the same simulation data as Figure 1. The first column of panels display the model (*grey*) and fitted (*black*) 21 cm PS, and the linear matter PS (*thick grey* line) at redshifts of $z = 6.5, 7.0, 7.5$ and 8.0 . The panels in the second column show the fitted (*black*) and model (*grey*) scale dependent bias. The anomalous power component of the fit is plotted in the third column. In the far right-hand panels we plot the difference between the model PS with and without baryons (*grey*), and the recovered PS with and without baryons (*black*), as described in the text. The *grey* error bars correspond to spherically averaged noise as described in Section 3. In each panel the vertical lines indicate the range of k values used for the fit.

and may be written

$$\Delta P_{21,N}(\vec{k}) = \left[\frac{T_{\text{sky}}^2}{\Delta\nu t_{\text{int}}} \frac{D^2 \Delta D}{n(k_{\perp})} \left(\frac{\lambda^2}{A_e} \right)^2 \right] \frac{1}{\sqrt{N_c}}, \quad (5)$$

where D is the co-moving distance to the centre of the survey volume which has a co-moving depth ΔD . Here $n(k_{\perp})$ is the density of baselines which observe a wave vector with transverse component k_{\perp} . Note that this factor ensures that k -modes which do not fit in the bandpass $\Delta\nu$ are not observable. N_c denotes the number of modes observed in a k -space volume d^3k . In terms of the k -vector components,

$N_c = 2\pi k_{\perp} \Delta k_{\perp} \Delta k_{\parallel} \mathcal{V} / (2\pi)^3$ where $\mathcal{V} = D\Delta D(\lambda^2/A_e)$ is the observed volume. The sample variance component of the noise is given by $\Delta P_{21,SV}(\vec{k}) = P_{21}(\vec{k})/\sqrt{N_c}$. The sensitivity will improve with the square root of the number of independent fields observed. The total noise may therefore be expressed by

$$\Delta P_{21}(k_{\perp}, k_{\parallel}, z) = \frac{\Delta P_{21,N}(k_{\perp}, k_{\parallel}, z) + \Delta P_{21,SV}(k_{\perp}, k_{\parallel}, z)}{\sqrt{N_{\text{fields}} B_{\text{tot}} / \Delta\nu}}. \quad (6)$$

Note that we have assumed complete foreground removal over a bandpass with width $\Delta\nu$ [see McQuinn et al. (2006)

for a discussion of the relationship between foreground removal and bandpass width]. In Section 4 we explore the effect of the choice of $\Delta\nu$ on the errors in the measurement of α_\perp and α_\parallel .

We assume the data is binned into 16 logarithmically spaced intervals with mid points in the range $0.05 \text{ Mpc}^{-1} \leq k_\perp, k_\parallel \leq 0.2 \text{ Mpc}^{-1}$. The resulting uncertainty on the spherically averaged PS is depicted as the grey error bars in the far right-hand panels of Figures 1 and 2. Wave numbers below this range would not fit within the nominal bandwidth of $\sim 8 \text{ MHz}$ at the redshifts of interest. Above 0.2 Mpc^{-1} the BAO signal becomes very weak and the matter PS may be non-linear. We assume that three fields are observed ($N_{\text{fields}} = 3$) for 1000 hrs each. Given the field of view at these redshifts, this would correspond to surveying a few per cent of the sky.

4 FITS TO 21 CM POWER SPECTRA

In this section we describe the results of fits to the modeled 21 cm PS using the parametrized forms in equations (3)–(4).

4.1 χ^2 minimization

We adopt the χ^2 function as an indicator for the “goodness of fit” of our model,

$$\chi^2(\vec{p}) = \sum_{i=1}^{n_\perp} \sum_{j=1}^{n_\parallel} \left[\frac{P_{21}(k_{\perp i}, k_{\parallel j}, z) - P_{21, \text{fit}}(\vec{p}, k_{\perp i}, k_{\parallel j}, z)}{\sigma_{ij}} \right]^2, \quad (7)$$

where $\sigma_{ij} = \Delta P_{21}(k_{\perp i}, k_{\parallel j}, z)$ and $\vec{p} \equiv \{p_i\} = (\alpha_\perp, \alpha_\parallel, b_0, b_1, b_2, b_3, c_0, c_1, c_2)$ is a vector containing the model parameters. The index i (j) refers to the n_\perp (n_\parallel) discrete values of k_\perp (k_\parallel) corresponding to each data bin (see Section 3). We restrict our fitting to the range $0.05 \text{ Mpc}^{-1} < k_\parallel, k_\perp < 0.2 \text{ Mpc}^{-1}$.

We have adapted the Numerical Recipes routines (Press et al. 1992) which implement the Levenberg-Marquardt technique to iteratively find the parameter set which minimizes the χ^2 function for a model which is non-linear in its parameters \vec{p} . In Figures 1 and 2 we show the resulting fits for the cases with a third order polynomial bias (black lines), with and without a quadratic anomalous power term respectively. The panels in the second column of Figure 1 (and the first column in Figure 2) show the fitted spherically averaged 21 cm PS as well as the linear matter PS. The panels in the third column of Figure 1 (and second column of Figure 2) show the fitted 21 cm bias. In Figure 2 the panels in the third column show the fitted AP term (note that the input term is zero since non-linear effects are not incorporated into the semi-numeric code we have used to generate the ionisation maps). The far right-hand panels in each of Figures 1 and 2 show the BAO component of the fitted PS, $B^2(k)D^2(z)P_1(k) + AP(k) - b_{21}^2(k)D^2(z)P_{1, \text{nb}}(k)$. The noise in the fitted BAO component is due to the noise in the model calculation of the bias b_{21} .

The fit to the 21 cm PS is very good in all cases, with slight discrepancies at the low- k end toward $z \sim 6.5$ for the case of no anomalous power. The inclusion of the AP reduces this discrepancy. When the anomalous power term is included there is a trade-off between the power in the 21 cm

PS associated with the bias B and that due to AP , indicating some degeneracy. However as we show in the next subsection, this degeneracy does not significantly bias the constraints on the BAO scale. It may of course be possible to alleviate the degeneracies between the bias and AP parameters by putting some physically/numerically motivated priors on the values of c_0, c_1 and c_2 .

4.2 Uncertainty in the measured BAO scale

After marginalising over the remaining fit parameters, we may interpret the errors in α_\perp and α_\parallel for our fits as the fractional uncertainties in the measurement of the transverse and line-of-sight BAO scales (Seo & Eisenstein 2005). The Fisher matrix \mathbf{F} is given by (Tegmark et al. 1997)

$$F_{ij} = \sum_{k=0}^{n_p} \sum_{l=0}^{n_p} \frac{\partial P_{21, \text{fit}}}{\partial p_i} \frac{\partial P_{21, \text{fit}}}{\partial p_j}, \quad (8)$$

where n_p is the dimension of \vec{p} and all derivatives are evaluated using the best-fitting \vec{p} . Since we expect the noise in 21 cm PS to be Gaussian, we may invoke the Cramer-Rao theorem to estimate the 1σ (68.3 per cent) confidence interval around the best-fitting values for α_\perp and α_\parallel from \mathbf{F} . Assuming that all other parameters are marginalised over this implies errors around the best-fitting values for α_\parallel and α_\perp are

$$\begin{aligned} \Delta\alpha_\perp &= (F_{11}^{-1})^{-1/2}, \\ \Delta\alpha_\parallel &= (F_{22}^{-1})^{-1/2}. \end{aligned} \quad (9)$$

In Figures 3 and 4 we plot the the best-fitting values of $\alpha_\perp, \alpha_\parallel$ and the associated 1σ error as calculated in equation (9) for several redshifts in the range $6.4 \leq z \leq 8$. Figure 4 assumes a fitted 21 cm PS that includes an anomalous power term, whereas the fitted PS used to generate Figure 3 does not. In each figure the grey horizontal line indicates the input value $\alpha_\perp = \alpha_\parallel = 1$. Note that the recovered values of α_\perp and α_\parallel are not within 1σ of the true values for $z \lesssim 6.7$, indicating that the scale dependent 21 cm bias introduces a systematic measurement error at these redshifts (i.e. our maximum-likelihood estimator is biased). The redshift $z \sim 6.7$ corresponds to the redshift below which the 21 cm bias becomes most strongly scale dependent in the range $0.05 \text{ Mpc}^{-1} < k < 0.2 \text{ Mpc}^{-1}$ for the reionisation model we have assumed. This systematic error is a result of the (relatively) low noise level in the 21 cm PS toward $z \sim 6.5$ combined with the increasingly strong evolution of the bias function within the fitted range of k -values. The statistical and systematic errors are each slightly larger when we include the extra parameters to required to describe the anomalous power (since the matrix \mathbf{F} is not diagonal). We note that our estimate of the attainable errors on the parameters α_\perp and α_\parallel are a minimum in the sense that (i) we have assumed perfect foreground removal across each bandpass with width 8 MHz for a total bandwidth of 32 MHz, and (ii) we have invoked the Cramer-Rao theorem regarding the minimum 1σ error on a parameter from the Fisher matrix of the best-fitting model.

The bandpass over which foreground removal can be performed may affect the errors on the model parameters, even for a fixed total bandpass B_{tot} , because the removal of foreground on larger scales allows for more of the strong

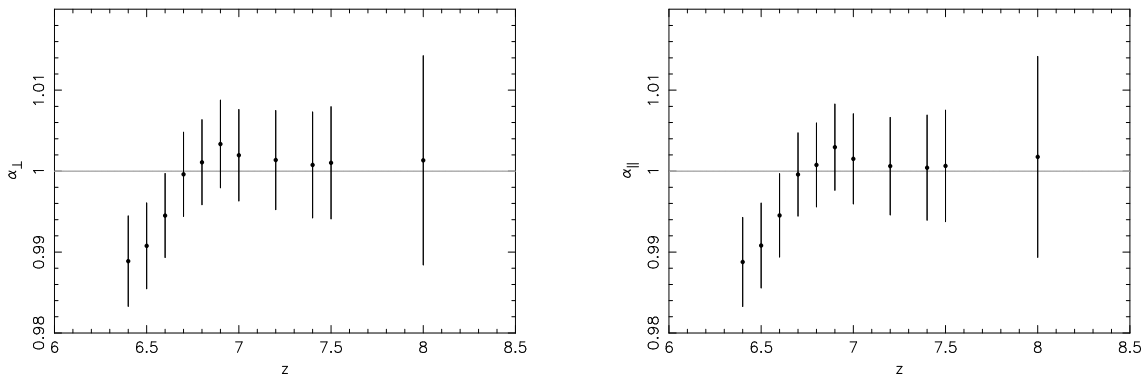


Figure 3. Fitted values and uncertainty for the parameters α_{\perp} (left) and α_{\parallel} (right) as a function of redshift using a fit with third-order polynomial bias and no anomalous power. The points indicate the recovered value of $\alpha_{\perp,\parallel}$ for input values $\alpha_{\perp,\parallel} = 1$. The error bars represent the 1σ (68.3 per cent) confidence interval as calculated using a Fisher matrix and marginalising over all the remaining fit parameters.

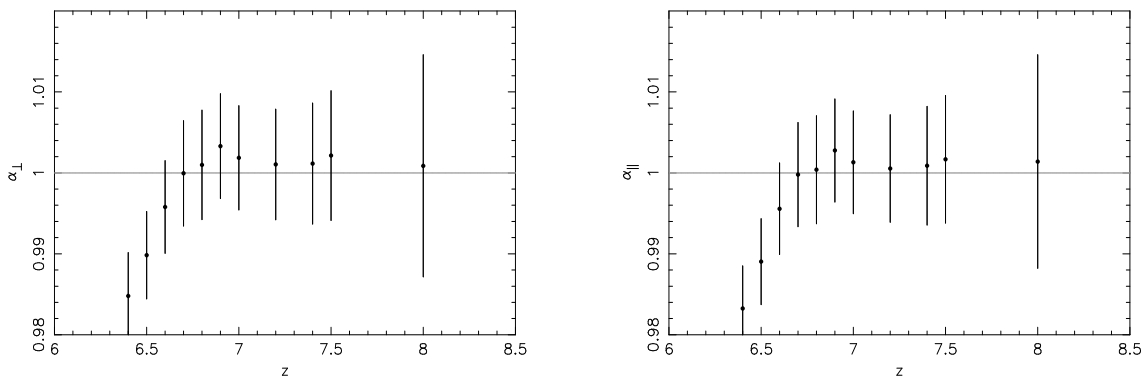


Figure 4. As per Figure 3, but using a fit with third-order polynomial 21 cm bias and quadratic anomalous power.

large-scale (small k) BAO peaks to be included in the fit. However we find that at the high redshifts that we are considering, increasing $\Delta\nu$ above 8 MHz has little effect on the errors in the recovered values of α_{\perp} and α_{\parallel} . On the other hand, we find that decreasing $\Delta\nu$ increases the statistical uncertainty in the recovered values of α_{\perp} and α_{\parallel} at all redshifts considered. Where the AP term was included we find that decreasing $\Delta\nu$ to 6 MHz also significantly increases the systematic error in the lowest redshift bin $z = 6.4$. In contrast, for the case with no AP term, decreasing the bandpass width actually reduces the systematic error in the lowest redshift bins. The latter effect arises because the lowest few k -bins lie in the region where the 21 cm bias is least well described by the polynomial fit at the end of reionisation (see the top panel of Figure 1).

The systematic component of the errors will be sensitive to the functional form chosen to describe the 21 cm PS. We find that increasing the order of the polynomial used to fit the bias to fourth-order reduces the systematic bias in the fitted values of α_{\perp} and α_{\parallel} at redshifts near $z \sim 6.5$ by up to ~ 0.5 per cent (with or without anomalous power, see Figures 5 and 6). At redshifts where the fit is unbiased in α_{\perp} or α_{\parallel} we find little effect on the size of the statistical errors (except at $z \sim 8$ in the case where anomalous power is included for which the statistical noise increases noticeably).

5 SUMMARY AND CONCLUSIONS

There has been recent interest in the utility of redshifted 21 cm fluctuations from the IGM as a probe of the mass PS at a range of redshifts (e.g. McQuinn et al. 2006; Bowman et al. 2006; Mao et al. 2008; Wyithe et al. 2008; Chang et al. 2007; Mao & Wu 2008). During the reionisation era ($z \gtrsim 6$), the appearance of HII regions generates scale dependence of the bias relating the 21 cm PS to the linear PS. In this paper we have set out to test the extent to which the scale dependence of the 21 cm bias will interfere with the ability to extract the BAO scale from the PS of 21 cm fluctuations.

We have utilised the results of semi-numerical models for the evolution of the ionised hydrogen distribution on large scales in order to construct an estimate for the 21 cm PS at high redshift. For a model in which the IGM is fully reionised by $z = 6$, and assuming the design parameters for a 10-fold expansion the the MWA, we find that the scale dependent 21 cm bias limits the precision, but not the accuracy, of measurements of the BAO scale in the window $6.7 < z < 8$. We parametrize the bias and anomalous power terms in the 21 cm PS as polynomials, and for the telescope design assumed, find errors on the line-of-sight and transverse BAO scales of $\lesssim 1.5$ per cent. At redshifts closer to the end of reionisation, the strong angular dependence of the 21 cm bias introduces systematic error in the BAO scale at a

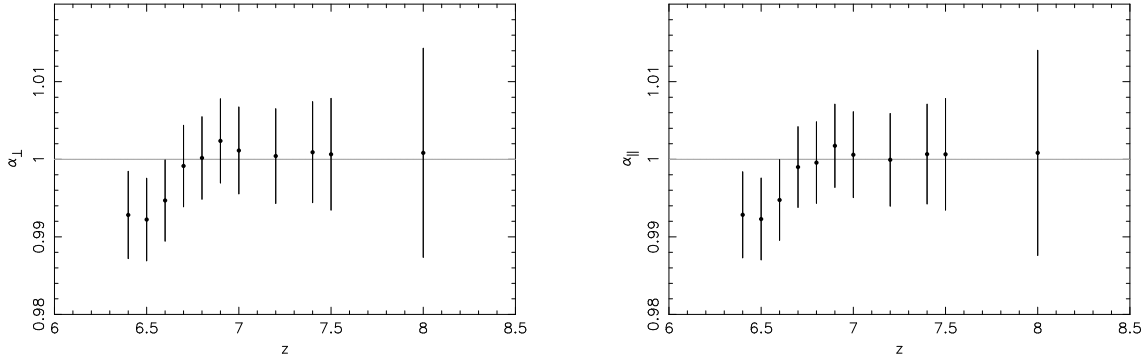


Figure 5. As per Figure 3, but using a fit with a fourth-order polynomial fit to the 21 cm bias and no anomalous power.

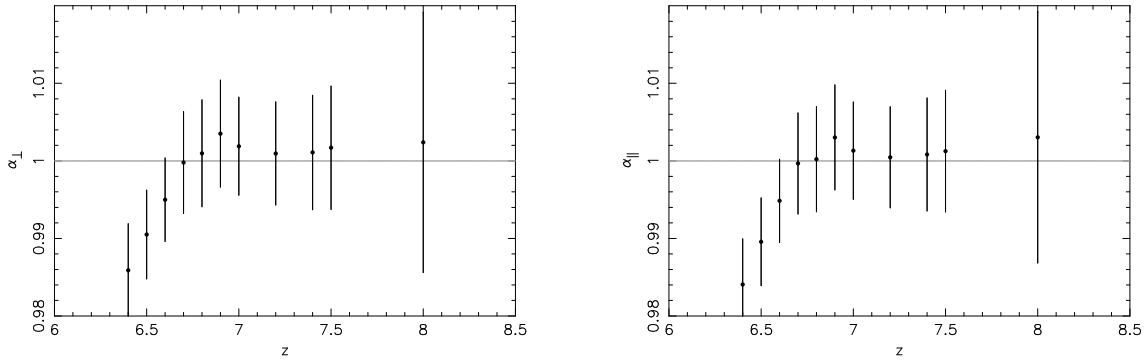


Figure 6. As per Figure 3, but using a fit with a fourth-order polynomial fit to the 21 cm bias and quadratic anomalous power.

level in excess of the statistical uncertainty. We find that the sensitivity of a low-frequency array to both the line-of-sight and transverse components of the BAO scale are very similar at each of the redshifts considered, and that this sensitivity decreases with increasing redshift.

A detailed analysis of the corresponding constraints on the dark energy equation of state is non-trivial and depends on the functional form assumed (Wyithe et al. 2008). We do not explore the translation of BAO scale to cosmological constraints in this paper. Such an analysis should include independent complementary constraints (e.g. from the CMB), and take account of uncertainties in, for example, the horizon scale (e.g. McQuinn et al. 2006; Mao et al. 2008). Simple estimates of the cosmological constraints from a high redshift BAO measurement were presented in Wyithe et al. (2008).

In a recent paper Mao et al. (2008) propose a parametrization of the 3d 21 cm PS including peculiar velocity effects which is motivated by the generic form expected for the ionisation PS and ionisation-matter PS. Our analysis of the accuracy with which the BAO scale may be recovered in the presence of a scale dependent 21 cm bias is complementary to their detailed discussion of the cosmological constraints available via the redshifted 21 cm PS. Mao et al. (2008) demonstrate that their parametrization can recover the ionisation PS constructed from simulations of reionisation and therefore can be used to constrain cosmological parameters from the 21 cm PS. Whilst they mention that their parametrization struggles to describe the high- k ionisation PS by a redshift of $z = 7$ when the ionisation PS become significantly scale dependent, this is not found to be

a problem up to the $k_{\max} = 0.2 \text{ Mpc}^{-1}$ that we consider in this paper. It would be interesting to see how well such a parametrization would perform at the end of reionisation in the wavelength range that we have used for our fits.

Our calculations of the constraints on the BAO scale from 21 cm intensity fluctuations are promising when compared to the expected performance of future galaxy surveys. Glazebrook & Blake (2005) show that a dedicated next-generation spectroscopic galaxy survey could measure the BAO scale to an accuracy of ~ 1 per cent for the transverse component at a redshift $z \sim 3.5$, with a slightly reduced sensitivity to the line-of-sight BAO scale. Limitations in the precision achievable arise due to the large number of galaxies needed to reduce the cosmic variance on the scales at which the BAO signal is expected ($\gtrsim 30 \text{ Mpc}$), combined with the decrease in the number of sufficiently luminous galaxies toward higher redshift. The accuracy with which the BAO scale may be measured via the 21 cm intensity PS is immune to both of these constraints because there is no need to resolve individual objects. Redshifted 21 cm measurements of the PS will instead be limited by cosmic variance owing to the finite size of the field of view, and sensitivity to individual modes owing to array configuration and finite collecting area. However we find that the PS of redshifted 21 cm fluctuations as measured by the MWA5000 could achieve constraints on the BAO scale at $z > 6$ that are comparable to the accuracy which will be available to future galaxy redshift surveys at $z \lesssim 3.5$.

In summary, one potential obstacle to measuring the BAO scale in 21 cm fluctuations during the reionisation era is the strongly scale dependent bias between the 21 cm and

mass PS that is produced by the appearance of large ionised regions. In this paper we have shown that the appearance of ionised regions during the reionisation epoch will not inhibit the measurement of the BAO scale during most of the reionisation era.

ACKNOWLEDGMENTS

KJR acknowledges the support and hospitality of the Department of Physics, University of Melbourne, and a visiting postgraduate Marie Curie Fellowship at MPA. The research was supported by the Australian Research Council (JSBW). PMG acknowledges the support of an Australian Postgraduate Award.

REFERENCES

- Angulo R. E., Baugh C. M., Frenk C. S., Lacey C. G., 2008, *MNRAS*, 383, 755
- Barkana R., Loeb A., 2005, *ApJ*, 624, L65
- Blake C., Glazebrook K., 2003, *ApJ*, 594, 665
- Bowman J. D., Morales M. F., Hewitt J. N., 2006, *ApJ*, 638, 20
- Chang T.-C., Pen U.-L., Peterson J. B., McDonald P., 2007, *ArXiv e-prints*, 0709.3672
- Cole S., Percival W. J., Peacock J. A., Norberg P., Baugh C. M., Frenk C. S., Baldry I., Bland-Hawthorn J., Bridges T., Cannon R., Colless M., Collins C., Couch W., Cross N. J. G., Dalton G., Eke V. R., De Propriis R., Driver S. P., Efstathiou G., Ellis R. S., Glazebrook K., Jackson C., Jenkins A., Lahav O., Lewis I., Lumsden S., Maddox S., Madgwick D., Peterson B. A., Sutherland W., Taylor K., 2005, *MNRAS*, 362, 505
- Corasaniti P.-S., Huterer D., Melchiorri A., 2007, *ArXiv e-prints*, 0701.433
- Croce M., Scoccimarro R., 2008, *Phys. Rev. D*, 77, 023533
- Eisenstein D., 2002, in *Astronomical Society of the Pacific Conference Series*, Vol. 280, *Next Generation Wide-Field Multi-Object Spectroscopy*, Brown M. J. I., Dey A., eds., pp. 35–+
- Eisenstein D. J., Hu W., Tegmark M., 1998, *ApJ*, 504, L57+
- Eisenstein D. J., Zehavi I., Hogg D. W., Scoccimarro R., Blanton M. R., Nichol R. C., Scranton R., Seo H.-J., Tegmark M., Zheng Z., Anderson S. F., Annis J., Bahcall N., Brinkmann J., Burles S., Castander F. J., Connolly A., Csabai I., Doi M., Fukugita M., Frieman J. A., Glazebrook K., Gunn J. E., Hendry J. S., Hennessy G., Ivezić Z., Kent S., Knapp G. R., Lin H., Loh Y.-S., Lupton R. H., Margon B., McKay T. A., Meiksin A., Munn J. A., Pope A., Richmond M. W., Schlegel D., Schneider D. P., Shimasaku K., Stoughton C., Strauss M. A., SubbaRao M., Szalay A. S., Szapudi I., Tucker D. L., Yanny B., York D. G., 2005, *ApJ*, 633, 560
- Furlanetto S. R., 2006, *MNRAS*, 371, 867
- Furlanetto S. R., Zaldarriaga M., Hernquist L., 2004, *ApJ*, 613, 16
- Geil P. M., Wyithe S., 2007, *ArXiv e-prints*, 0708.3716
- Giannantonio T., Scranton R., Crittenden R. G., Nichol R. C., Boughn S. P., Myers A. D., Richards G. T., 2008, *ArXiv e-prints*, 0801.4380
- Glazebrook K., Blake C., 2005, *ApJ*, 631, 1
- Hu W., Haiman Z., 2003, *Phys. Rev. D*, 68, 063004
- Komatsu E., Dunkley J., Nolta M. R., Bennett C. L., Gold B., Hinshaw G., Jarosik N., Larson D., Limon M., Page L., Spergel D. N., Halpern M., Hill R. S., Kogut A., Meyer S. S., Tucker G. S., Weiland J. L., Wollack E., Wright E. L., 2008, *ArXiv e-prints*, 0803.0547
- Mao X.-C., Wu X.-P., 2008, *ApJ*, 673, L107
- Mao Y., Tegmark M., McQuinn M., Zaldarriaga M., Zahn O., 2008, *ArXiv e-prints*, 0802.1710
- McDonald P., Eisenstein D. J., 2007, *Phys. Rev. D*, 76, 063009
- McQuinn M., Lidz A., Zahn O., Dutta S., Hernquist L., Zaldarriaga M., 2007a, *MNRAS*, 377, 1043
- , 2007b, *MNRAS*, 377, 1043
- McQuinn M., Zahn O., Zaldarriaga M., Hernquist L., Furlanetto S. R., 2006, *ApJ*, 653, 815
- Mesinger A., Furlanetto S., 2007, *ApJ*, 669, 663
- Page L., Nolta M. R., Barnes C., Bennett C. L., Halpern M., Hinshaw G., Jarosik N., Kogut A., Limon M., Meyer S. S., Peiris H. V., Spergel D. N., Tucker G. S., Wollack E., Wright E. L., 2003, *ApJS*, 148, 233
- Percival W. J., Cole S., Eisenstein D. J., Nichol R. C., Peacock J. A., Pope A. C., Szalay A. S., 2007, *MNRAS*, 381, 1053
- Press W. H., Teukolsky S. A., Vetterling W. T., Flannery B. P., 1992, *Numerical recipes in C. The art of scientific computing*. Cambridge: University Press, —c1992, 2nd ed.
- Seljak U., Zaldarriaga M., 1996, *ApJ*, 469, 437
- Seo H.-J., Eisenstein D. J., 2003, *ApJ*, 598, 720
- , 2005, *ApJ*, 633, 575
- , 2007, *ApJ*, 665, 14
- Simpson F., Bridle S., 2006, *Phys. Rev. D*, 73, 083001
- Spergel D. N., Bean R., Doré O., Nolta M. R., Bennett C. L., Dunkley J., Hinshaw G., Jarosik N., Komatsu E., Page L., Peiris H. V., Verde L., Halpern M., Hill R. S., Kogut A., Limon M., Meyer S. S., Odegard N., Tucker G. S., Weiland J. L., Wollack E., Wright E. L., 2007, *ApJS*, 170, 377
- Tegmark M., Taylor A. N., Heavens A. F., 1997, *ApJ*, 480, 22
- Trac H., Cen R., 2007, *ApJ*, 671, 1
- Wyithe J. S. B., Loeb A., Geil P. M., 2008, *MNRAS*, 383, 1195
- Wyithe J. S. B., Morales M. F., 2007, *MNRAS*, 379, 1647
- Zahn O., Lidz A., McQuinn M., Dutta S., Hernquist L., Zaldarriaga M., Furlanetto S. R., 2007, *ApJ*, 654, 12